Available online at www.sciencedirect.com
SCIENCE DIRECT
Journal of Magnetic Resonance 181 (2006) 191–198
JMR Journal of Magnetic Resonance
www.elsevier.com/locate/jmr

Relaxation and diffusion of perfluorocarbon gas mixtures with oxygen for lung MRI

Yulin V. Chang [a,*], Mark S. Conradi [a,b]

[a] Department of Physics, Washington University, St. Louis, MO 63130, USA
[b] Department of Radiology, Washington University, St. Louis, MO 63110, USA

Received 22 December 2005; revised 29 March 2006
Available online 16 May 2006

Abstract

We report measurements of free diffusivity D_0 and relaxation times T_1 and T_2 for pure C_2F_6 and C_3F_8 and their mixtures with oxygen. A simplified relaxation theory is presented and used to fit the data. The results enable spatially localized relaxation time measurements to determine the local gas concentration in lung MR images, so the free diffusivity D_0 is then known. Comparison of the measured diffusion to D_0 will express the extent of diffusion restriction and allow the local surface-to-volume ratio to be found.

Keywords: Perfluorocarbon gas; Hyperpolarized gas; Lung; Diffusion; Relaxation

1. Introduction

Hyperpolarized ^{3}He gas MR imaging has developed rapidly over the last several years for probing porous materials, especially lungs [1–4]. Spin density images display the spatial distribution of the inspired gas and have been used to understand several lung diseases [5,6]. Maps of ^{3}He self-diffusion in emphysema show large increases in diffusion in regions of airway expansion and alveolar wall destruction, allowing the severity of the disease to be imaged [7–9]. Measurements of the microscopic anisotropy of restricted diffusion allow the average radius of acinar airways to be determined non-invasively [10]. Tagging of longitudinal spin magnetization has been used to measure restricted diffusion over longer distances (centimeters) and is believed to be sensitive to the collateral pathways that become important in emphysema [11]. Relaxation of ^{3}He spin magnetization by paramagnetic oxygen has been exploited to image the partial pressure of O_2 throughout the lungs [12]. This has been developed into a method to image the local ratio of ventilation to perfusion (blood flow, which absorbs O_2 from the gas) [13].

Despite these successes with hyperpolarized ^{3}He, it remains primarily a research tool without widespread clinical implementation. We believe a major reason for this is the expense of the laser-based polarizing apparatus and the skilled personnel to maintain it. Thus, several research groups are exploring the potential of ordinary (Boltzmann polarized) ^{19}F MR of perfluorinated gases such as SF_6, C_2F_6, and C_3F_8 [14–19]. We note that the first such report was with CF_4 by Lauterbur and colleagues [20] approximately 20 years ago. These gases gain signal-to-noise (S/N) by having 4 to 6 equivalent ^{19}F spins per molecule and a short T_1 to allow rapid signal averaging. Crucially, there are essentially no endogenous ^{19}F spins in the body that could interfere with the gas signals. The perfluorinated gases can be mixed with 20% oxygen for continuous breathing with only a 20% decrease in ^{19}F spin density and similar changes in T_1 and T_2. Thus, human lungs can be filled and imaged with 80% concentration perfluorinated gas; by comparison most human ^{3}He studies are restricted by gas cost to 0.3–1.0 L of ^{3}He in a total lung volume of approximately 6 L. (A typical ^{3}He exam uses two doses of 0.5 L STP ^{3}He each; the current price of this gas is

* Corresponding author.
E-mail address: ychang@wustl.edu (Y.V. Chang).

1090-7807/$ - see front matter © 2006 Elsevier Inc. All rights reserved.
doi:10.1016/j.jmr.2006.04.003

$135. By comparison, C_2F_6 costs $0.85/STP liter. A recirculating ventilator system and subject might contain 10 L, so $8.50 worth of gas. This recirculating gas could be used for several measurements: ADC, T_1 and spin density.) In addition, 20% oxygen reduces T_1 of ^{3}He to 10 s [21], limiting single bolus measurements to approximately this time. This time currently limits the fraction of the lung that can be covered in live humans for images of diffusion anisotropy [10] and long-range restricted diffusion [11]. The time limit also prevents any measurements at steady-state breathing. Thus, MR imaging with ^{19}F has the potential to become a practical, low-cost replacement for at least some applications of hyperpolarized ^{3}He.

Our group has recently shown that diffusion of C_2F_6 and C_3F_8 gases is substantially restricted in excised normal human donor lungs such that the measured diffusivity is approximately 50% of the free diffusivity D_0 [22–24]. In excised severely emphysematous lungs, the ^{19}F diffusion is less restricted (approximately 90% of D_0), demonstrating that perfluorocarbon (PFC) gas imaging can readily distinguish healthy and emphysematous lung regions. Clearly, to assess the extent of restriction to gas diffusion one needs to know the free diffusivity D_0 of the gas, for comparison to the diffusivity measured in the lung. Because different gas species have different masses and collision cross sections, the free self-diffusivity of the PFC gas depends on the gas concentration. In lungs, where some regions are poorly ventilated and O_2 is continuously taken up by the blood in the alveolar walls, the concentration of the gas and its ^{19}F free diffusivity D_0 will not be equal to those of the inspired PFC–oxygen gas mixture and will vary throughout the lungs [22]. This work addresses the determination of D_0 for C_2F_6 and C_3F_8 mixtures with oxygen, from measurements of T_1 or T_2. We believe the relaxation time T_2 of SF_6 is too short to allow measurements of D in the present-generation human scanners [22,25], so SF_6 is not included in this study. A report of T_1 for more fluorinated gases (including C_2F_6), pure and mixed with other gases, has appeared [26].

Mitra et al. [27] have shown that the restricted diffusivity $D(t)$ measured over time duration t can be used to determine the (local) surface area to gas volume ratio, S/V. For sufficiently short times, where only a small fraction of gas molecules strike the walls in time t, $\sqrt{D_0 t} \ll (S/V)^{-1}$,

$$\frac{D(t)}{D_0} \cong 1 - A\sqrt{D_0 t}\frac{S}{V}, \tag{1}$$

where the dimensionless constant A is different for narrow gradient pulses and for wide pulses (e.g., static gradients) [28]. Here the walls are assumed to be perfectly reflective, a good approximation for these non-water-soluble PFC gases. For C_2F_6 and C_3F_8, the low free diffusivity D_0 makes Eq. (1) valid for practical diffusion times t [25], approximately 5–10 ms. A spatially resolved measurement of lung S/V would be very useful to understanding emphysema in general and in individual patients. In emphysema, acinar airway expansion and tissue destruction result in larger airspaces, increased diffusion (less restriction), and decreased S/V ratio [29,30] (currently measured by light microscopy after tissue fixation and staining). Restricted diffusion measurements by MR could follow the progression of emphysema non-invasively. One simple implementation of Eq. (1) to obtain S/V would involve measurement of $D(t)$ at a single time t and knowledge of D_0 by determination of the gas concentration. Use of Eq. (1) with two very different values of diffusion time t may be impractical, with the available gradient strength limiting the shortest t values and T_2 limiting the longest values of t.

Whether for a simple qualitative assessment of the extent of restriction to diffusion or a quantitative measure of S/V, one must know D_0 in each imaging voxel. Most of the background gases in living lungs are O_2, N_2, CO_2 and H_2O. In the in vivo experiments we envision, one will provide the subject a mixture of PFC gas and O_2. Any N_2 present initially will be washed out over time with steady state breathing. The partial pressure of CO_2 released in a human lung is about 40 mm Hg [31], only 5% of the total gas pressure. The saturated H_2O pressure at 37 C is 47 mm Hg [32], about 6% of the total pressure. Thus CO_2 and H_2O will make up at most 11% of all the gas in the lung. In addition, their effects on D_0, T_1, and T_2 of PFC gases will be of the same magnitude as the effects of the similarly sized O_2 molecules (in PFC gases, the direct effect of the paramagnetic moment of O_2 is small compared to the effect through collisions on the molecular angular momentum lifetime τ_J of the PFC molecules). Thus, it suffices to know the dependences of D_0, T_1, and T_2 on the concentration of the PFC gas in mixtures with oxygen; the effects of other gases (CO_2 and H_2O) have been neglected in our study. We note that the mean free path of the PFC gases is much, much smaller than the mean distance between walls, so T_1 and T_2 are negligibly sensitive to collisions with walls. Measurement of T_1 or T_2 thus determines the gas concentration and the free diffusivity D_0. We believe this approach to be superior to determining the gas concentration from the amplitude of the spin signal in each voxel, because of inhomogeneity of the rf field and sensitivity of the rf coil and because of variations in the fraction of each imaging voxel which is gas space, not tissue.

We report here measurements of T_1, T_2, and D_0 for C_2F_6 and C_3F_8 at various pressures and for mixtures of each PFC gas with O_2 at constant pressure. The measurements at two field strengths permit the data to be fitted to analytical expressions for T_1 and T_2 that are valid over the range of pressures and concentrations useful for lung imaging and for typical imaging field strengths.

2. Methods

Gas pressures were measured using an absolute pressure transducer (Kavlico, P650-30A-BIA) with the range from 0 to 2 atm. The pressure transducer was calibrated at vacuum (less than 20 mtorr) and at 75.25 cm Hg, as determined

by a barometer. The gauge output was assumed to be linear with pressure, as specified by the manufacturer.

All samples were flame-sealed in standard-wall Pyrex tubes of 1 cm ID. Sample tubes were all necked in advance to make sealing easier and faster. For pure samples of C_2F_6 (99.9% purity) and C_3F_8 (99% purity), both from Scott Specialty Gases, we filled the sample tube to various desired pressures directly from the gas bottle after evacuating the tube. For mixed samples we first mixed C_2F_6 or C_3F_8 with O_2 (Matheson, 99.9% purity) in a stainless steel gas cylinder of 75 cc or 150 cc, with beads inside. Then the cylinder was removed and shaken for one minute to better mix the gases. The sample tube was filled with the mixed gas from the cylinder at 0.94 atm at 22 C for all mixtures for easy flame-sealing, as the narrow neck collapses under outside atmosphere pressure when heated with a torch.

All relaxation measurements were performed in an Oxford superconducting 4.4 T solenoid or a Varian electromagnet at 1.5 T, the latter of which is similar to the field of many human MRI scanners. The frequencies of ^{19}F at these fields are 175.59 and 59.88 MHz, respectively. Room temperature shims were used in both magnets to provide a more uniform field at the sample location. Data were taken using a laboratory-built spectrometer, which includes a 25 W transmitter power amplifier (ENI). A typical 90° pulse is 35 μs at 4.4 T and 5 μs at 1.5 T. Both rf coils are about 1.5 cm in diameter and 3 cm in length.

Laboratory-written software was used to acquire and analyze data. Data analysis was done in the time domain.

T_1 was measured with an inversion-recovery sequence. The rf phase of the inversion pulse was alternated $(x, -x)$ to cancel the small FID resulting from the imperfect π pulse. The signal S as a function of the delay time t between the two rf pulses is

$$S(t) = S_\infty(1 - Be^{-t/T_1}). \tag{2}$$

The value of B is 2 for complete inversion of the spin magnetization; here B was typically 1.86. S_∞ is the fully recovered signal strength and was typically obtained at $t = 300$ ms, which is 15 times the longest measured T_1. Seven or eight different delay values were used. $S(t)$ was obtained by integrating the FID in the real channel after baseline and phase correction. For C_3F_8, T_1 reported here refers to the six CF_3 fluorine atoms, which were put on exact resonance. The other two F atoms are shifted by 48 ppm [22]; their off-resonance signal does not contribute to the time integral used for data analysis.

We used the standard $\frac{\pi}{2} - \tau - \pi$ spin–echo sequence for the T_2 measurements. The following 4-step phase cycling scheme was used to eliminate signals other than the spin echo: $\frac{\pi}{2}$ pulse: $x, -x, x, -x$; π pulse: x, x, y, y; receiver: $+, -, -, +$. The echo amplitude $S(2\tau)$, taken as the magnitude of the echo, decays with pulse spacing τ as

$$S(2\tau) = S_0e^{-2\tau/T_2}. \tag{3}$$

Diffusion of the gases was measured with a constant field gradient in the 4.4 T magnet. Constant gradients yield a very precise and easily measured value of the gradient amplitude G without eddy-current, rise-time or undershoot compensation issues. However, since only the dependence of echo amplitude upon τ is available (varying G causes additional echo-amplitude changes from changes in the spin-signal bandwidth), the data must be corrected for T_2 decay. Diffusion data were taken using the same spin–echo pulse sequence as in T_2 experiments, with τ values from 0.5 to 7.0 ms. Here the echo amplitude $S(2\tau)$ is

$$S(2\tau) = S_0e^{-2\tau/T_2}e^{-2\gamma^2G^2D\tau^3/3}. \tag{4}$$

A plot of $(\ln(S(2\tau)) + 2\tau/T_2)$ vs. τ^3 yields a slope of $-\frac{2}{3}\gamma^2G^2D$, from which D is calculated. T_2 values for correcting the echo-amplitudes were obtained by measurements of spin echoes in the absence of a gradient.

The gradient coil was a Maxwell pair of AWG-22 enamelled copper wire on the aluminum can of the probe with 8.0 cm OD. It has 40 turns on each half, the centers of which are spaced 6.8 cm apart. The calculated gradient is 2.05 Gauss/cm/Amp, from the coil geometry and the Biot-Savart formula. The gradient amplitude was calibrated using a spherical bulb (Wilmad) filled with water. We determined the inner radius r of the bulb by weighing the water inside to determine the volume of the bulb. In the presence of a constant gradient G, the Fourier transform of the echo signal is a resonance of full width Δf (measured at the baseline),

$$\Delta f = \gamma_H(2r)G/2\pi. \tag{5}$$

We used several values of current up to 1 Amp and plotted linewidths as a function of the current. The best linear fit is 2.08 Gauss/cm/Amp, and this value was used for all diffusion measurements. During the experiments the current was monitored by reading the voltage across a precision 0.01 Ω resistor. The typical current we used for diffusion measurements was 0.4 Amp, which caused negligible heating of the probe and sample.

To study the temperature dependence of the relaxation and diffusion over a narrow temperature range, selected samples were also measured at 37 C (physiological temperature) and 48 C in the 4.4 T magnet. For these experiments a heater-resistor together with a temperature controller was used to blow warm air across the sample. The sample temperature was independently monitored by a type T thermocouple. For the 22 C measurements at 4.4 T, ambient air was blown across the sample.

3. Theory of relaxation and diffusion

For gases with ^{19}F nuclear spins, the dominant interaction for spin relaxation is the spin–rotation interaction, coupling the nuclear spins to local magnetic fields produced by rotation of the molecule. The ^{19}F–^{19}F dipolar interactions are weak by comparison, which may be inferred by comparing the relaxation times of (say) CH_4 and CF_4:

despite the dipolar interactions between ^{19}F spins being slightly smaller than those in the smaller molecule CH_4, the relaxation time T_1 at a given density is much smaller for CF_4 [33,34].

For C_2F_6, there are two modes of overall dumbell molecular rotation; in addition, the CF_3 groups can rotate about the C—C bond. The situation is even more complicated for the nonlinear molecule C_3F_8. A correct description of these systems involves using separate spin–rotation coupling constants and correlation times τ_J for the physically distinct modes of rotation. However, our intention is not a first-principles analysis; rather, we seek to characterize T_1 and T_2 over the range of pressures and NMR frequencies relevant to MR imaging with these gases.

Thus, we make the simplification that a single spin–rotation interaction with a single correlation time τ describes these systems. This results in a manageable set of parameters to describe the data; a more exact treatment is not warranted by the data, which are mainly (but not entirely) in the $\omega\tau \ll 1$ limit. Following the theory for linear molecules [35,36],

$$\frac{1}{T_1} = M_2 \frac{2\tau}{1+\omega^2\tau^2}, \tag{6}$$

where ω is the spin precession angular frequency. The molecular Zeeman frequency ω_J is generally small compared to the spin frequency and has been neglected here. The second moment M_2 expresses the squared strength of the spin–rotation coupling and is expected to vary linearly with absolute temperature according to the equipartition theorem [35]. With the same restrictions, the transverse relaxation rate is

$$\frac{1}{T_2} = M_2\left(\tau + \frac{\tau}{1+\omega^2\tau^2}\right). \tag{7}$$

For $\omega\tau \ll 1$, T_1 and T_2 are thus equal.

At a given temperature, the rate $1/\tau$ of angular momentum-changing collisions will be linear in the gas density or pressure P, as these gases are well-approximated as ideal gases. In general, in a gas PFC–oxygen mixture with partial pressures P_F and P_O for the PFC and oxygen components, respectively,

$$\frac{1}{\tau} = K_F P_F + K_O P_O. \tag{8}$$

Here K_F and K_O are constants reflecting the sizes and reduced masses of the binary FF and OF systems. Combining Eqs. (6)–(8) we obtain

$$T_1 = \frac{1+\omega^2/(K_F P_F + K_O P_O)^2}{2M_2}(K_F P_F + K_O P_O), \tag{9}$$

and

$$T_2 = \frac{K_F P_F + K_O P_O}{M_2\left(1+\frac{1}{1+\omega^2/(K_F P_F + K_O P_O)^2}\right)}. \tag{10}$$

In the fast collision limit, $\omega^2\tau^2 \ll 1$, so T_1 and T_2 can be approximated by a single expression

$$T_1 = T_2 = \frac{K_F P_F + K_O P_O}{2M_2}. \tag{11}$$

For a fixed total pressure P, $P_O = P - P_F$, and introducing x as the concentration of PFC, $x \equiv P_F/P$, Eq. (11) becomes

$$T_1 = T_2 = \frac{P}{2M_2}((K_F - K_O)x + K_O). \tag{12}$$

Thus, at low frequency, a linear variation of T_1 and T_2 with concentration x is predicted.

For pure gases where $x = 1$, the general results (9) and (10) become

$$T_1 = \frac{K_F}{2M_2}P + \frac{\omega^2}{2M_2 K_F}\frac{1}{P}, \tag{13}$$

and

$$T_2 = \frac{K_F P}{M_2\left(1+\frac{1}{1+\omega^2/(K_F P)^2}\right)}. \tag{14}$$

For self-diffusion of the PFC component in a binary gas mixture with oxygen, the reciprocal of the self-diffusion coefficient D varies linearly with the partial pressures as [37]

$$\frac{1}{D(x,P)} = \frac{P_F}{\mathcal{D}_F} + \frac{P_O}{\mathcal{D}_O}, \tag{15}$$

where $\mathcal{D}_F$ is the value of D for pure PFC at $P = 1$ atm and $\mathcal{D}_O$ is the value of D for PFC at infinite dilution in oxygen at $P = 1$ atm. The units of $\mathcal{D}_F$ and $\mathcal{D}_O$ are atm cm^2/s. In terms of the fractional concentration x of PFC and total pressure P,

$$\frac{1}{D(x,P)} = \frac{xP}{\mathcal{D}_F} + \frac{(1-x)P}{\mathcal{D}_O} = P\left(x\left(\frac{1}{\mathcal{D}_F} - \frac{1}{\mathcal{D}_O}\right) + \frac{1}{\mathcal{D}_O}\right). \tag{16}$$

Thus, a linear variation with concentration x is expected for $1/D$ of PFC at a constant total pressure. For pure PFC at different pressures, Eq. (16) can be simplified by setting $x = 1$,

$$\frac{1}{D(1,P)} = \frac{P}{\mathcal{D}_F}. \tag{17}$$

3.1. Temperature dependence

The temperature dependence of the parameters ($M_2, K_F, K_O, \mathcal{D}_F$ and $\mathcal{D}_O$) will give us a full description of how relaxation and diffusion change with temperature. Here we are interested in only the narrow range from 22 C to 37 C (physiological temperature). As stated above, M_2 is expected to be linear with the absolute temperature, thus

$$M_2 \propto T. \tag{18}$$

The temperature dependence of K_F and K_O can be derived from the experimental data. Our variable-temperature experiments were carried out at a constant density

(with sealed samples), where pressure is proportional to temperature and the relaxation is approximately in the fast collision regime. We find that

$$T_1 \propto T^{\alpha}, \tag{19}$$

where $\alpha = -1.4$ (see Section 4). Then from Eqs. (12) and (18) we obtain

$$K_F, K_O \propto T^{\alpha}. \tag{20}$$

The variable-temperature diffusion measurements were performed similarly at constant density, so P is again proportional to T. We find that all the data are in satisfactory agreement with

$$D \propto T^{\beta}, \tag{21}$$

with $\beta = 0.8$ (see Section 4). Referring to Eq. (15), this yields the temperature dependence of parameters $\mathcal{D}_F$ and $\mathcal{D}_O$,

$$\mathcal{D}_F, \mathcal{D}_O \propto T^{\beta+1}. \tag{22}$$

4. Results and discussion

All T_1 and diffusion data at 22 C are plotted in Figs. 1–4 (T_2 data are available graphically and all data are tabulated in the supplementary material). We fit all the T_1 and T_2 data using the appropriate formulas presented in the above section with 3 parameters for each gas: M_2, K_F and K_O; $\mathcal{D}_F$ and $\mathcal{D}_O$ were chosen to fit the diffusion data. These parameters are listed in Table 1 for data at 22 C and Table 2 for data at 37 C.

Fig. 1 shows T_1 of the pure PFC gases at 22 C as a function of pressure at two measurement-frequencies. The

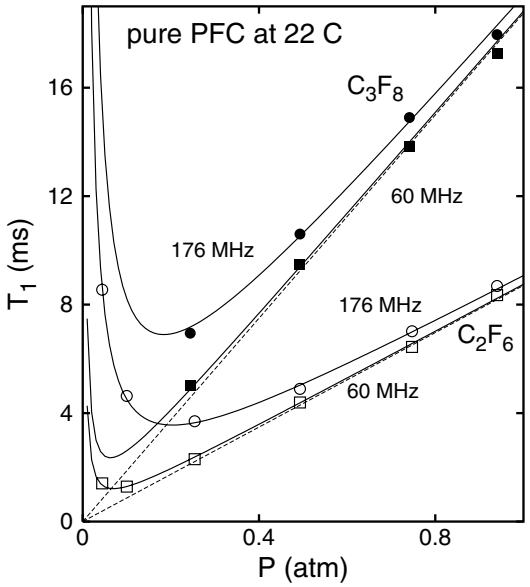

Fig. 1. T_1 for pure C_3F_8 (solid symbols) and C_2F_6 (open symbols) gases at 22 C. Data are presented for 60 MHz (squares) and 176 MHz (circles). The solid curves are fits to the data using Eq. (13) with the parameters M_2 and K_F listed in Table 1. The dashed lines are the predictions for zero frequency.

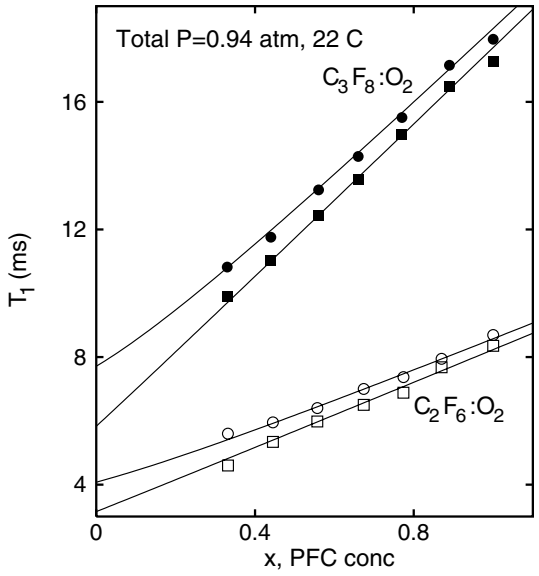

Fig. 2. T_1 of C_3F_8 and C_2F_6 gas mixtures with oxygen at 22 C and a total pressure of 0.94 atm as a function of PFC concentration x. Data are shown for 60 MHz (squares) and 176 MHz (circles). The curves are fits using Eq. (9) with the parameters in Table 1. The present data are used to determine K_O, using M_2 and K_F values previously determined from the pure gas data, as in Fig. 1. The 60 MHz data are nearly linear in x.

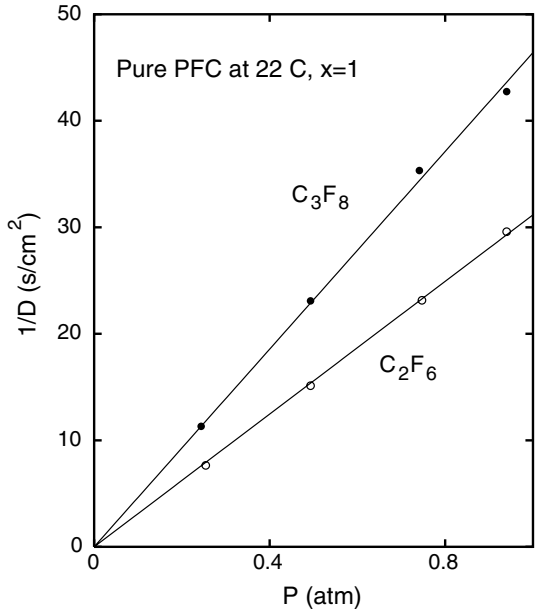

Fig. 3. Reciprocal of the diffusivity for pure C_3F_8 and C_2F_6 gases at 22 C as a function of pressure P. The lines are best fits of Eq. (17) to the data, forced to pass through the origin; these determine the parameters $\mathcal{D}_F$ in Table 1. The larger and more massive C_3F_8 molecule has a lower diffusivity at a given pressure.

dashed lines are the expected linear T_1 behaviors when the external field is zero ($\omega \to 0$ limit), from Eq. (13). We note that T_1 of C_3F_8 is almost twice as long as T_1 of C_2F_6 at each pressure. Otherwise, the T_1's of these two gases vary quite similarly: at 60 MHz they are both linear functions of pressure until $P < 0.2$ atm, where they

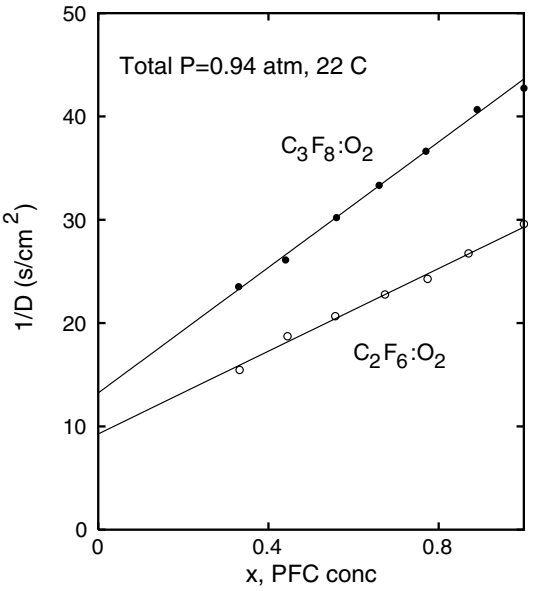

Fig. 4. Reciprocal diffusivity of C_3F_8 and C_2F_6 gas mixtures with oxygen at 22 C and a total pressure of 0.94 atm as a function of PFC concentration x. The lines are linear fits to the data according to Eq. (16) with the parameters in Table 1. The present data are used to determine $\mathcal{D}_O$, using the previously determined values of $\mathcal{D}_F$, as in Fig. 3.

noticeably deviate from the straight line and reach minima at about 0.07 atm. At 176 MHz the minima occur at a higher pressure, about 0.2 atm, in accordance with Eq. (13). For pressures near 0.6–1.0 atm, the frequency dependence of T_1 is small but not negligible, demonstrating that $\omega\tau < 1$ here. The parameters M_2 and K_F in Table 1 were determined for each pure gas from least-squares fits of Eq. (13) to the data of Fig. 1.

Fig. 2 presents T_1 of PFC–oxygen mixtures at 22 C and a constant total pressure (0.94 atm) as a function of concentration x of the PFC component. Clearly T_1 decreases with decreasing x and increasing oxygen concentration. According to Eq. (12), this shows that $K_O < K_F$, as expected for the smaller scattering cross-section of oxygen–PFC encounters compared to PFC–PFC encounters. At 60 MHz, T_1 varies nearly linearly with concentration, even when x is small, so Eq. (12) is a very good approximation in this case. The fractional variation of T_1 between 60 and 176 MHz is larger at low x where T_1 is smaller, as expected from Eq. (9). The parameters K_O in Table 1 were taken from least-squares fits of Eq. (9) to the T_1 data of Fig. 2.

Fig. 3 shows the linear dependence of $1/D$ upon pressure for pure PFC's at 22 C, as predicted by Eq. (17). Both lines have been forced to pass through the origin, implying infinite diffusivities at zero pressure, as expected. At a given pressure, C_3F_8 always has a lower D than C_2F_6 because it is a larger and heavier molecule. Least-squares linear fits to Eq. (17) were used to determine the values of $\mathcal{D}_F$ in Table 1. Fig. 4 displays linear variations of $1/D$ with PFC concentration x at 22 C and a constant total pressure P of 0.94 atm, as predicted by Eq. (16). Because O_2 is a smaller and lighter molecule with a smaller scattering cross-section, we have $\mathcal{D}_O > \mathcal{D}_F$, implying that $1/D$ should be an increasing function of x, in agreement with the measured data. The parameters $\mathcal{D}_O$ in Table 1 were obtained by least-squares fits of Eq. (16) to the data of Fig. 4.

Four samples of each gas, three mixed with oxygen, were measured again at both 37 C and 48 C. A log–log plot (not presented) of all T_1 versus temperature data shows an average α of -1.4 ± 0.3 (see Eq. (19)). This result agrees closely with previous studies of the similar molecules SF_6 and CF_4 [34,38], where α is -1.5. We thus estimated K_F and K_O at 37 C in Table 2 according to Eq. (20) using $\alpha = -1.5$, from the 22 C values in Table 1. We have plotted the T_1 data at 37 C of pure PFC samples and PFC–O_2 mixtures together with the predictions of Eqs. (9) and (13) with the parameters of Table 2. The agreement between data and calculation (not shown) is as good as in Figs. 1 and 2 (at 22 C).

The same procedure for diffusion yields $\beta = 0.8 \pm 0.2$ in Eq. (22). The approximation of constant scattering cross-section would yield β of 0.5 [39]. We obtained $\mathcal{D}_F$ and $\mathcal{D}_O$ at 37 C using $\beta = 0.8$ in Eq. (22); these values appear in Table 2. The 37 C diffusion data and the curves calculated from Eq. (15) with the Table 2 parameters show the same level of agreement as in Figs. 3 and 4 (at 22 C).

In practice, our goal is to use restricted PFC diffusion to study lungs and lung disease. Thus it is necessary to provide the imaging subjects a PFC–oxygen mixture. The dependence of T_1 upon PFC concentration at a known total pressure, as given by Eq. (9) and the parameters listed in Table 1 or 2, will allow the PFC concentration to be

Table 1
Fitting parameters at 22 C

Gas	M_2 (10^{11} s^{-2})	K_F (10^9 atm^{-1} s^{-1})	K_O (10^9 atm^{-1} s^{-1})	$\mathcal{D}_F$ (atm cm^2/s)	$\mathcal{D}_O$ (atm cm^2/s)
C_2F_6	3.10 ± 0.05	5.4 ± 0.1	2.0 ± 0.1	0.0321 ± 0.0005	0.101 ± 0.005
C_3F_8	1.6 ± 0.1	6.0 ± 0.1	1.9 ± 0.1	0.0216 ± 0.0004	0.071 ± 0.002

Table 2
Fitting parameters at 37 C

Gas	M_2 (10^{11} s^{-2})	K_F (10^9 atm^{-1} s^{-1})	K_O (10^9 atm^{-1} s^{-1})	$\mathcal{D}_F$ (atm cm^2/s)	$\mathcal{D}_O$ (atm cm^2/s)
C_2F_6	3.3 ± 0.1	5.0 ± 0.1	1.9 ± 0.1	0.0351 ± 0.0005	0.110 ± 0.006
C_3F_8	1.7 ± 0.1	5.6 ± 0.1	1.8 ± 0.1	0.0235 ± 0.0001	0.077 ± 0.001

determined in each pixel, from spatially revolved T_1 measurements. The concentration will, in turn, allow the free diffusivity to be determined from Eq. (16) and Table 1 or 2.

Comparing C_2F_6 with C_3F_8, we notice that under the same condition the latter always has a longer T_1. The measured T_2 values are close (90% or more) to the T_1 values for pressures above 0.6 atm for pure PFC or any concentration x of PFC–oxygen mixtures at a total pressure of 0.94 atm. In most available 1.5 T human scanners the echo time (te) may need to be as long as 10 ms for diffusion measurements due to the limited available gradient strength. Thus, at (say) 60% concentration x, the C_2F_6 signal would be strongly attenuated by its T_2 of about 6 ms. By comparison, the 12 ms T_2 of C_3F_8 at the same concentration is longer so that less signal attenuation will result.

The diffusion coefficients of the two PFC gases studied here are much smaller than that of ^{3}He, which is 0.88 cm^2/s in air. Using $l_{He} = \sqrt{2Dt}$, the characteristic diffusion length at a diffusion time t of 2 ms (typical for ^{3}He) is 0.6 mm. This is greater than the average acinar airway radius r (about 0.35 mm) of human lung [40], meaning that the ^{3}He diffusion in human lung is strongly restricted. On the other hand, for PFC, the characteristic diffusion length l_F will be smaller. For C_3F_8 at concentration $x = 0.7$ in a C_3F_8–O_2 mixture at 0.94 atm total pressure, D_0 will be 0.028 cm^2/s so l_F will be 0.17 mm for a diffusion time of 5 ms (typical for ^{19}F work). Thus, the diffusion of C_3F_8 in this mixture will be less restricted. With the free diffusion coefficient of this mixture from Fig. 4 or Eq. (16) with the parameters of Table 1 or 2, the measured restricted diffusion will allow the lung S/V to be determined, since the small diffusivity of this gas places it in the lightly restricted regime (Eq. (1)). Moreover the free diffusion can be adjusted by varying the gas concentration according to Fig. 4 at the expense of S/N. Adjustment of the gas mixture to increase the free diffusivity may be applied to S/V measurements of lungs with severe emphysema, as the very small S/V would otherwise yield a nearly unrestricted diffusivity.

5. Conclusion

Perfluorinated gases show promise for replacement of hyperpolarized ^{3}He in some of its applications, especially diffusion MR imaging of the lungs. A simplified theory of spin–rotation relaxation with 3 parameters has been employed to model T_1 and T_2 data for C_2F_6 and C_3F_8 gases and their mixtures with oxygen. The variation of free diffusivity D_0 has been measured and used to determine 2 parameters for a simple kinetic theory model. Thus, the measurements and parameters presented here will allow spatially resolved measurements of T_1 or T_2 to determine the local gas concentration. In turn, they will yield the free diffusion of the gas in the lung, which is crucial for quantitative assessment of the extent of restriction to diffusion and for determination of a local surface-area-to-volume ratio. Such measurements should provide a clear description of the extent of lung airway expansion and tissue destruction in emphysema.

Acknowledgments

We appreciate D.S. Gierada for suggesting this project. We are grateful to R.E. Jacob, J.C. Woods, and D.A. Yablonskiy for helpful discussions. Special thanks go to J.J.H Ackerman for reading the manuscript and giving valuable comments. The NMR work on the 4.4 T magnet used the RF probe built by Daniel Sinkovits. We thank Scott Specialty Gases for supplying C_3F_8 gas. The work was supported by the GEMI fund (Gas Enabled Medical Innovation).

Appendix A. Supplementary data

Supplementary data associated with this article can be found, in the online version, at doi:10.1016/j.jmr.2006.04.003.

References

[1] H. Middleton, R.D. Black, B. Saam, G.D. Cates, G.P. Cofer, B. Guenther, W. Happer, L.W. Hedlund, G.A. Johnson, K. Juvan, J. Swartz, MR imaging with hyperpolarized ^{3}He gas, Magn. Reson. Med. 33 (1995) 271–275.

[2] B. Saam, D.A. Yablonskiy, D.S. Gierada, M.S. Conradi, Rapid imaging of hyperpolarized gas using EPI, Magn. Reson. Med. 42 (1999) 507–514.

[3] X.J. Chen, H.E. Möller, M.S. Chawla, G.P. Cofer, B. Driehuys, L.W. Hedlund, G.A. Johnson, Spatially resolved measurements of hyperpolarized gas properties in the lung in vivo. Part 1: diffusion coefficient, Magn. Reson. Med. 42 (1999) 721–728.

[4] H.E. Möller, X.J. Chen, B. Saam, K.D. Hagspiel, G.A. Johnson, T.A. Altes, E.E. de Lange, H-U. Kauczor, MRI of the lungs using hyperpolarized noble gases, Magn. Reson. Med. 47 (2002) 1029–1051.

[5] T.A. Altes, P.L. Powers, J. Knight-Scott, G. Rakes, T.A.E. Platts-Mills, E.E. Lange, B.A. Alford, J.P. Mugler III, J.R. Brookeman, Hyperpolarized ^{3}He MR lung ventilation imaging in asthmatics: preliminary findings, J. Magn. Reson. Imaging 13 (2001) 378–384.

[6] L.F. Donnelly, J.R. MacFall, H.P. McAdams, J.M. Majure, J. Smith, D.P. Frush, P. Bogonad, H.C. Charles, C.E. Ravin, Cystic Fibrosis: combined hyperpolarized ^{3}He-enhanced and conventional proton MR imaging in the lung–preliminary observations, Radiology 212 (1999) 885–889.

[7] J.C. Leawoods, D.A. Yablonskiy, B. Saam, D.S. Gierada, M.S. Conradi, Hyperpolarized ^{3}He gas production and MR imaging of the lung, Concepts Magn. Reson. 13 (2001) 277–293.

[8] M. Salerno, E.E. de Lange, T.A. Altes, J.D. Truwit, J.R. Brookman, J.P. Mugler, Emphysema: hyperpolarized helium 3 diffusion MR imaging of the lungs compared with spirometric indexes-initial experience, Radiology 222 (2002) 252–260.

[9] B. Saam, D.A. Yablonskiy, V.D. Kodibagkar, J.C. Leawoods, D.S. Gierada, J.D. Cooper, S.S. Lefrak, M.S. Conradi, MR imaging of diffusion of ^{3}He gas in healthy and diseased lungs, Magn. Reson. Med. 44 (2000) 174–179.

[10] D.A. Yablonskiy, A.L. Sukstanskii, J.C. Leawoods, D.S. Gierada, G.L. Brehthorst, S.S. Lefrak, M.S. Conradi, Quantitative in vivo assessment of lung microstructure at the alveolar level with hyperpolarized ^{3}He diffusion MRI, Proc. Natl. Acad. Sci. USA 99 (2002) 3111–3116.

[11] J.C. Woods, D.A. Yablonskiy, K. Chino, T.S.K. Tanoli, J.D. Cooper, M.S. Conradi, Magnetization tagging decay to measure long-range

^{3}He diffusion in healthy and emphysematous canine lungs, Magn. Reson. Med. 51 (2004) 1002–1008.
[12] A.J. Deninger, B. Eberle, M. Ebert, T. Grobmann, W. Heil, H.U. Kauczor, L. Lauer, K. Markstaller, E. Otten, J. Schmiedeskamp, W. Schreiber, R. Surkau, M. Thelen, N. Weiler, Quantification of regional intrapulmonary oxygen partial pressure evolution during apnea by ^{3}He MRI, J. Magn. Reson. 141 (1999) 207–216.
[13] R.R. Rizi, J.E. Baumgardner, M. Ishii, Z.Z. Spector, J.M. Edvinsson, A. Jalali, J. Yu, M. Itkin, D.A. Lipson, W. Gefter, Determination of regional V_A/Q by hyperpolarized ^{3}He MRI, Magn. Reson. Med. 52 (2004) 65–72.
[14] D.O. Kuethe, A. Caprihan, E. Fukushima, R.A. Waggoner, Imaging lungs using inert fluorinated gases, Magn. Reson. Med. 38 (1998) 85–88.
[15] D.O. Kuethe, A. Caprihan, H.M. Gach, I.J. Lowe, E. Fukushima, Imaging obstructed ventilation with NMR using inert fluorinated gases, J. Appl. Physiol. 88 (2000) 2279–2286.
[16] W.G. Schreiber, B. Eberle, S. Laukemper-Ostendorf, K. Markstaller, N. Weiler, A. Schloz, K. Bürger, C.P. Heussel, M. Thelen, H.U. Kauczor, Dynamic ^{19}F-MRI of pulmonary ventilation using sulfur hexafluoride (SF_6) gas, Magn. Reson. Med. 45 (2001) 605–613.
[17] Jesús Ruiz-Cabello, José Manuel Pérez-Sánchez, Rigoberto Pérez de Alejo, Ignacio Rodríguez, Nicolás González-Mangado, Germán Peces-Barba, Manuel Cortijo, Diffusion-weighted ^{19}F-MRI of lung periphery: influence of pressure and air-SF_6 composition on apparent diffusion coefficients, Respir. Physiol. Neurobiol. 148 (2005) 43–56.
[18] N. Adolphi, D. Kuethe, First T_1 images of inert fluorinated gases in lungs, in: 7th International Conference on Magnetic Resonance Microscopy, Snowbird, UT, USA, 2003.
[19] S.D. Beyea, S.L. Codd, D.O. Kuethe, E. Fukushima, Studies of porous media by thermally polarized gas NMR: current status, Magn. Reson. Imaging 21 (2003) 201–205.
[20] P.A. Rinck, S.B. Petersen, P.S. Lauterbur, NMR imaging of fluorine-containing substances: 19-fluorine ventilation and perfusion studies, Fortschr Röntgenstr 140 (1984) 239–243.
[21] B. Saam, W. Happer, H. Middleton, Nuclear relaxation of ^{3}He in the presence of O_2, Phys. Rev. A 52 (1995) 862–865.
[22] R.E. Jacob, Y.V. Chang, C.K. Choong, A. Biehals, D.Z. Hu, J. Zheng, D.A. Yablonskiy, J.C. Woods, D.S. Gierada, M.S. Conradi, ^{19}F MR imaging of ventilation and diffusion in excised lungs, Magn. Reson. Med. 54 (2005) 577–585.
[23] M.S. Conradi, D.A. Yablonskiy, J.C. Woods, D.S. Gierada, R.E. Jacob, Y.V. Chang, C.K. Choong, A.L. Sukstanskii, T. Tanoli, S.S. Lefrak, J.D. Cooper, ^{3}He Diffusion MRI of the lung, Acad. Radiol. 12 (11) (2005) 1406–1413.
[24] M.S. Conradi, B. Saam, D.A. Yablonskiy, J.C. Woods, Hyperpolarized ^{3}He and perfluorocarbon gas diffusion MRI of lungs, Prog. Nuc. Mag. Reson. Spectrosc. 48 (1) (2006) 63–83.
[25] M.S. Conradi, M.A. Bruns, A.L. Sukstanskii, S.S. Gross, J.C. Leawoods, Feasibility of diffusion-NMR surface-to-volume measurements tested by calculations and computer simulations, J. Magn. Reson. 169 (2004) 196–202.
[26] D.O. Kuethe, T. Pietrass, V.C. Behr, Inert fluorinated gas T_1 calculator, J. Magn. Reson. 177 (2005) 212–220.
[27] P.P. Mitra, P.N. Sen, L.M. Schwartz, Short-time behavior of the diffusion coefficient as a geometrical probe of prorous media, Phys. Rev. B 47 (1993) 8565–8574.
[28] T.M. de Swiet, P.N. Sen, Decay of nuclear magnetization by bounded diffusion in a constant field gradient, J. Chem. Phys. 100 (1994) 5597–5604.
[29] H.O. Coxson, R.M. Rogers, K.P. Whittall, Y. D'Yachkova, P.D. Pare, F.C. Sciurba, J.C. Hogg, A quantification of the lung surface area in emphysema using computed tomography, Am. J. Respir. Crit. Med. 159 (1999) 851–856.
[30] G.L. Snider, J. Kleinerman, W. Thurlbech, Z.H. Bengali, The definition of emphyzema. Report of a National Heart, Lung and Blood Institute, Division of Lung Diseases Workshop, Am. Rev. Respir. Dis. 132 (1985) 182–185.
[31] John B. West, Respiratory Physiology—The Essentials, fifth ed., Williams & Wilkins, Baltimore, USA, 1995, p. 30.
[32] Handbook of Chemistry and Physics, 85th edition, CRC press, 2004, pp. 6–10.
[33] S. Rajan, K. Lalita, S.V. Babu, Intermolecular potentials from NMR data: II. CH_4, CF_4 and SiF_4, Can. J. Phys. 53 (1975) 1631–1635.
[34] R.L. Armstrong, E. Tward, Spin-Lattice relaxation in dilute gases. II. ^{19}F relaxation in CF_4 and SiF_4, J. Chem. Phys. 48 (1968) 332–334.
[35] A. Abragam, The Principles of Nuclear Magnetism, Oxford, UK, 1973, p. 318.
[36] R.L. Armstrong, Nuclear magnetic relaxation effects in polyatomic gases, Magn. Reson. Rev. 12 (1987) 91–135.
[37] C.R. Wilke, Diffusional properties of multicomponent gases, Chem. Eng. Progress 42 (2) (1950) 95–104.
[38] J.A. Courtney, R.L. Armstrong, A nuclear spin relaxation study of the spin- rotation interaction in spherical top molecules, Can. J. Phys. 50 (1971) 1252–1261.
[39] F. Reif, Fundamentals of statistical and thermal physics, McGraw-Hill, NY, 1965, [chapter 12].
[40] B. Haefeli-Bleuer, E.R. Weibel, Morphometry of the human pulmonary acinus, Anat. Rec. 220 (1988) 401–414.